Research Square

Preprints are preliminary reports that have not undergone peer review.
They should not be considered conclusive, used to inform clinical practice,
or referenced by the media as validated information.

Coastal Erosion Hotspots and Shoreline Vulnerability Zonation along the Northern Persian Gulf: A Regional Assessment Using Landsat, DSAS, and Spatial Statistics

Mostafa Ahmadi
Khorramshahr University of Marine Science and Technology
Morteza Bakhtiari
mortezabakhtiari62@gmail.com

Khorramshahr University of Marine Science and Technology
Arezoo Soleimany
Malayer University

Research Article

Keywords: Coastal erosion, Shoreline-change vulnerability, Hotspot analysis, Landsat, Coastal conservation, Persian Gulf

Posted Date: November 10th, 2026

DOI: https://doi.org/10.21203/rs.3.rs-11411570/v1

License: This work is licensed under a Creative Commons Attribution 4.0 International License.
Read Full License

Additional Declarations:
No competing interests reported.

Highlights

Landsat and DSAS mapped shoreline dynamics along the northern Persian Gulf.

Moran's I confirmed strong spatial clustering of shoreline change indicators.

Getis-Ord Gi* detected two erosion hotspots and one accretion-dominated zone.

Hotspot outputs were translated into shoreline vulnerability and priority zones.

The framework supports regional marine coastal monitoring and management.

Coastal Erosion Hotspots and Shoreline Vulnerability Zonation along the Northern Persian Gulf: A Regional Assessment Using Landsat, DSAS, and Spatial Statistics

Article type: Research Paper

Abstract

Coastal erosion and shoreline instability are major environmental concerns in low-lying and sediment-sensitive coastal zones, particularly where long-term field monitoring data are limited. This study develops an integrated framework for detecting coastal erosion hotspots and zoning shoreline vulnerability along the northern Persian Gulf using multi-temporal Landsat imagery, the Digital Shoreline Analysis System (DSAS), and spatial statistical techniques. Shoreline positions between 1993 and 2023 were extracted from Landsat 5, 7, 8, and 9 images using the Tasseled Cap Wetness component, and shoreline change was quantified along 350 shore-normal transects at 50-m intervals. Three DSAS-derived indicators, including Net Shoreline Movement (NSM), End Point Rate (EPR), and Linear Regression Rate (LRR), were calculated to assess shoreline displacement, annual change rate, and long-term trend. The results indicate pronounced spatial heterogeneity along the study coast, with NSM values ranging from -1159.84 to +965.38 m and LRR values ranging from -44.46 to +36.01 m yr^-1. The mean values of NSM, EPR, and LRR were -132.92 m, -4.44 m yr^-1, and -4.84 m yr^-1, respectively, indicating an overall dominance of shoreline retreat. Global Moran's I values for NSM, EPR, and LRR ranged from 0.862 to 0.865, confirming strong and statistically significant spatial autocorrelation in shoreline change patterns. Getis-Ord Gi* hotspot analysis identified two main erosion hotspots, mainly corresponding to transects 204-220 and 294-393, and a major accretion hotspot between transects 406-490. These spatial clusters were subsequently used to support shoreline vulnerability zonation and to distinguish high-priority erosion zones, relatively stable segments, and accretion-dominated areas. The findings demonstrate that integrating DSAS outputs with spatial statistics provides a more robust and management-oriented approach than conventional rate-based shoreline change assessment. The proposed framework can support regional coastal monitoring, risk-based shoreline management, and the prioritisation of erosion-control measures in data-scarce coastal regions of the Persian Gulf.

Keywords: Coastal erosion; Shoreline vulnerability; Hotspot analysis; Landsat; Persian Gulf

1. Introduction

Coastal zones are among the most dynamic and environmentally sensitive interfaces between terrestrial and marine systems. Shoreline position is continuously modified by the interaction of waves, tides, currents, sediment supply, sea-level variations, extreme events, and human interventions. These processes often produce complex patterns of erosion and accretion that vary considerably over short spatial distances. In low-lying and sediment-sensitive coastal environments, shoreline retreat can threaten coastal settlements, port facilities, aquaculture ponds, transportation corridors, wetlands, and natural habitats. Therefore, reliable monitoring of shoreline changes and the identification of erosion-prone coastal segments are essential for environmental assessment, coastal planning, and risk-based shoreline management.

Remote sensing and geographic information systems (GIS) have become widely used tools for shoreline monitoring because they provide repeated, synoptic, and cost-effective observations over long time periods. Among available satellite datasets, Landsat imagery is particularly valuable for multi-decadal shoreline change assessment due to its long archive, moderate spatial resolution, and global coverage. Previous studies have demonstrated the usefulness of satellite-based shoreline extraction methods for detecting long-term coastal changes, especially where continuous field measurements are limited. Spectral water indices and transformation-based approaches, such as the Normalized Difference Water Index (NDWI), Modified Normalized Difference Water Index (MNDWI), and Tasseled Cap Wetness component, have been widely applied to distinguish land-water boundaries and extract shoreline positions in different coastal environments (Boak & Turner, 2005; Fisher et al., 2016; Chen et al., 2019).

The Digital Shoreline Analysis System (DSAS) is one of the most commonly used tools for quantifying shoreline change. It enables the calculation of statistical indicators such as Net Shoreline Movement (NSM), End Point Rate (EPR), and Linear Regression Rate (LRR), which describe shoreline displacement, annual rate of change, and long-term shoreline trend, respectively. These indicators have been applied extensively in coastal erosion and accretion studies around the world. Studies such as Sunder et al. (2017), Kumar Das et al. (2021), Abdul Maulud et al. (2022), Thomas et al. (2023), and Colak (2024) have shown that DSAS-based metrics are effective for detecting shoreline retreat, shoreline advancement, and temporal changes in coastal morphology. However, many DSAS-based investigations remain primarily focused on reporting transect-based values, mean erosion rates, or general shoreline change trends.

Previous shoreline change studies can generally be grouped into several methodological directions. A first group has focused on shoreline definition, shoreline extraction, and the uncertainty associated with land-water boundary detection from remotely sensed imagery. These studies have emphasised the importance of image pre-processing, sensor resolution, spectral index selection, tidal conditions, and shoreline definition in reducing positional uncertainty (Boak & Turner, 2005; Fisher et al., 2016; Sun et al., 2023). A second group has applied multi-temporal satellite imagery and DSAS-based indicators to quantify shoreline displacement and rates of erosion or accretion in different coastal environments, including deltas, open sandy coasts, estuaries, lagoons, and semi-enclosed coastal systems (Zeinali et al., 2017; Abdul Maulud et al., 2022; Darwish & Smith, 2023; Sekar et al., 2024). These studies have contributed significantly to the understanding of long-term shoreline dynamics, but their outputs have often remained descriptive or rate-based.

A third group of studies has examined the role of natural and anthropogenic drivers in controlling shoreline instability. Natural factors such as wave exposure, tidal currents, sediment supply, sea-level variation, coastal slope, and geomorphological setting can strongly influence shoreline response. At the same time, human interventions, including port development, jetties, breakwaters, shoreline hardening, land reclamation, aquaculture expansion, and changes in coastal land use, can modify sediment transport pathways and intensify erosion or accretion in adjacent coastal segments (Gittman et al., 2015; Darwish & Smith, 2023; Khakhim et

al., 2024). These studies indicate that shoreline change is rarely spatially uniform and that erosion-prone areas often occur as localised clusters controlled by the interaction of morphology, hydrodynamics, sediment availability, and human activities.

More recently, shoreline change research has moved toward advanced modelling and integrated analytical approaches. Some studies have combined satellite image time series with machine learning, deep learning, data fusion, or predictive models to improve shoreline extraction accuracy and forecast future shoreline positions (Khurram et al., 2025; Nylen et al., 2025; Zorlu & Kusak, 2025). These approaches have expanded the analytical capability of shoreline monitoring studies. Nevertheless, predictive modelling is not always necessary or feasible, particularly in data-scarce coastal regions where the primary management need is not only to forecast future shoreline positions but also to identify current erosion hotspots, accretion clusters, and shoreline segments requiring priority intervention.

Despite these advances, two important research gaps remain. First, many shoreline change studies still treat DSAS-derived indicators mainly as numerical descriptors of erosion or accretion, rather than as spatial variables that can be statistically analysed to detect organised shoreline behaviour. As a result, spatial clustering, hotspot formation, and the non-random distribution of erosion and accretion may remain insufficiently explored. Second, relatively few studies have transformed NSM, EPR, and LRR outputs into spatially explicit erosion hotspot maps and shoreline vulnerability zones that can directly support environmental monitoring and coastal management. This limitation is important because a coastline may show a moderate average retreat rate while containing specific segments that experience severe and persistent erosion. Conversely, adjacent segments may show strong accretion or relative stability. Therefore, relying only on mean values or isolated transect-based statistics may obscure the actual spatial structure of shoreline instability.

Spatial statistical techniques provide a suitable framework for overcoming this limitation. Global spatial autocorrelation measures, such as Moran's I, can be used to determine whether shoreline change indicators are randomly distributed or spatially clustered along a coastline (Moran, 1950; Anselin, 1995). In addition, local hotspot analysis methods, such as Getis-Ord Gi*, can identify statistically significant clusters of high or low values (Getis & Ord, 1992; Ord & Getis, 1995). When applied to DSAS-derived shoreline change indicators, these techniques can distinguish erosion hotspots, accretion-dominated clusters, stable zones, and transitional shoreline segments. Integrating DSAS outputs with spatial statistics therefore allows shoreline change studies to move beyond conventional rate calculation toward a more management-oriented assessment of coastal instability and vulnerability.

The northern coast of the Persian Gulf is an environmentally important and morphologically diverse coastal region. It includes open muddy and sandy coasts, tidal inlets, shallow intertidal flats, coastal wetlands, ports, aquaculture ponds, and human-modified shorelines. These characteristics create favourable conditions for spatially heterogeneous shoreline behaviour. The coastal stretch between Khor-e Seh Deyreh and Bandar Genaveh is a representative example of such conditions. In this sector, tidal inlets and intertidal flats coexist with open coastlines and human interventions, leading to contrasting patterns of erosion, accretion, and relative stability over short distances. Despite the environmental and economic importance of this coastal zone, there is still a need for an integrated assessment that links long-term shoreline monitoring with erosion hotspot detection and shoreline vulnerability zonation.

The present study addresses this gap by developing an integrated framework for coastal erosion hotspot assessment and shoreline vulnerability zonation along the northern Persian Gulf. Multi-temporal Landsat images from 1993 to 2023 were used to extract shoreline positions based on the Tasseled Cap Wetness component. The DSAS tool was then applied to calculate NSM, EPR, and LRR along shore-normal transects.

Unlike conventional shoreline change studies that mainly report change rates, this research integrates DSAS-derived indicators with spatial statistical analyses, including Moran's I and Getis-Ord Gi*, to evaluate spatial autocorrelation and identify erosion-accretion hotspots. The results are further used to classify the coastline into vulnerability zones and management-priority segments.

The novelty of this study lies in transforming conventional DSAS shoreline change outputs into a spatially explicit regional marine coastal monitoring framework. Rather than merely calculating shoreline retreat and advancement rates, the study combines multi-decadal satellite-based shoreline monitoring, DSAS-derived shoreline change indicators, spatial autocorrelation analysis, hotspot detection, and GIS-based vulnerability zonation. This integrated approach provides a practical basis for identifying high-risk erosion zones, accretion-dominated areas, relatively stable shoreline segments, and priority areas for coastal management in a data-scarce coastal region of the Persian Gulf.

The specific objectives of this study are to:

- extract multi-temporal shoreline positions along the northern Persian Gulf using Landsat imagery from 1993 to 2023;
- quantify shoreline displacement and change rates using NSM, EPR, and LRR indicators;
- evaluate whether shoreline change indicators exhibit statistically significant spatial autocorrelation using Moran's I;
- identify erosion and accretion hotspots using Getis-Ord Gi* analysis; and
- develop a GIS-based shoreline vulnerability zonation framework for identifying management-priority coastal segments.

2. Materials and Methods

2.1. Study area

The study area is located along the northern coast of the Persian Gulf, extending between Khor-e Seh Deyreh and Bandar Genaveh. This coastal sector is part of the Bushehr Province coastline and is characterised by a combination of open coasts, tidal inlets, shallow intertidal flats, muddy coastal zones, and human-modified shoreline segments. The coexistence of natural coastal features and anthropogenic interventions has created a highly heterogeneous shoreline system in which erosion, accretion, and relatively stable segments occur over short alongshore distances.

The geographical location of the study area, including its position within Bushehr Province and the detailed coastal segment between Khor-e Seh Deyreh and Bandar Genaveh, is shown in Figure 1.

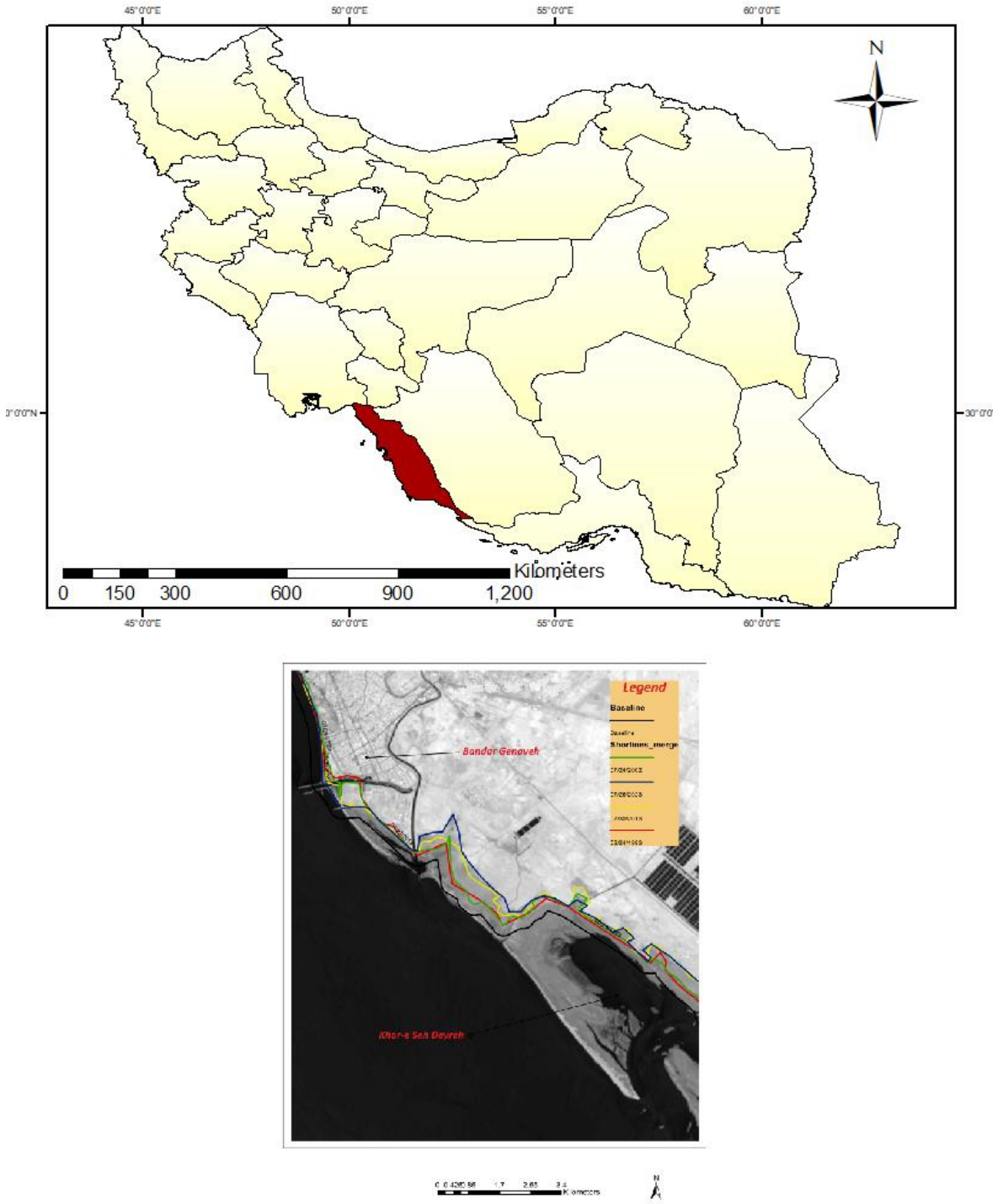


Figure 1. Location of the study area along the Khor-e Seh Deyreh-Bandar Genaveh coast, Bushehr Province, Northern Persian Gulf.

The eastern part of the study area is influenced by tidal inlets and low-energy depositional environments, whereas parts of the western and open-coast sections are more exposed to wave action and longshore sediment transport processes. In addition, coastal structures, aquaculture ponds, small piers, and human land-use changes have locally modified sediment transport pathways and shoreline configuration. These characteristics make the Khor-e Seh Deyreh-Bandar Genaveh coast an appropriate case for investigating coastal erosion

hotspots and shoreline vulnerability using satellite-based monitoring, DSAS-derived shoreline change indicators, and spatial statistical analysis.

2.2. Satellite data and image pre-processing

Multi-temporal Landsat satellite images were used to monitor shoreline changes over the period 1993-2023. The dataset included images acquired by Landsat 5 TM, Landsat 7 ETM+, Landsat 8 OLI, and Landsat 9 OLI/TIRS sensors. Landsat imagery was selected because of its long-term archive, moderate spatial resolution, and suitability for multi-decadal shoreline monitoring in coastal regions where continuous field observations are limited.

All satellite images were obtained from the United States Geological Survey archive as surface reflectance products. Radiometric and atmospheric corrections were therefore based on standard USGS processing procedures. Images with minimum cloud contamination over the coastal zone were selected, and cloud-affected pixels were excluded using the quality assessment bands. To ensure comparability between different acquisition dates and sensors, the images were visually checked and geometrically aligned before shoreline extraction. False-colour composites and reference imagery were used to support visual quality control of the extracted land-water boundary.

2.3. Shoreline extraction using Tasseled Cap Wetness

Shoreline extraction was carried out using a spectral index-based approach. The Tasseled Cap Wetness component was applied to enhance the discrimination between land and water surfaces, particularly in muddy and shallow intertidal coastal environments. The wetness component is sensitive to surface moisture and is therefore useful for delineating the land-water boundary in coastal zones affected by tidal flats, fine-grained sediments, and shallow water conditions.

For each selected Landsat image, the Tasseled Cap Wetness layer was generated and then classified into land and water classes using threshold-based separation. The resulting binary raster layers were converted into vector shoreline positions. After vectorisation, all extracted shorelines were visually inspected and manually corrected where necessary to remove obvious classification errors caused by tidal flats, wet sediments, cloud shadows, or local spectral confusion. The final extracted shorelines were then used as input layers for DSAS-based shoreline change analysis.

2.4. DSAS-based shoreline change analysis

Shoreline change analysis was performed using the Digital Shoreline Analysis System (DSAS) in the ArcGIS environment (Himmelstoss et al., 2021). A baseline was created landward of the extracted shorelines and approximately parallel to the general orientation of the coast. Shore-normal transects were then generated from the baseline toward the shoreline positions.

Based on the DSAS output table used in this study, the Khor-e Seh Deyreh-Bandar Genaveh coastal sector included 350 transects, corresponding to transect IDs 201 to 550. The transects were spaced at 50-m intervals along the baseline. This spacing provided a sufficiently detailed representation of alongshore variability in shoreline behaviour and enabled the identification of localised erosion and accretion clusters.

For each transect, four DSAS-derived shoreline change indicators were extracted:

Shoreline Change Envelope (SCE) represents the maximum distance among all shoreline positions intersecting a given transect, regardless of direction. It describes the total spatial envelope of shoreline variability.

$$SCE_i = \max(D_{i,t}) - \min(D_{i,t})$$

where D_i,t is the shoreline distance measured along transect i at time t.

Net Shoreline Movement (NSM) measures the net displacement between the oldest and most recent shoreline positions.

$$NSM_i = D_{i,t_latest} - D_{i,t_oldest}$$

In this study, negative NSM values indicate shoreline retreat or erosion, while positive values indicate shoreline advancement or accretion.

End Point Rate (EPR) calculates the annual rate of shoreline change between the oldest and most recent shoreline positions.

$$EPR_i = NSM_i / (t_latest - t_oldest)$$

Linear Regression Rate (LRR) estimates the long-term shoreline change trend by fitting a least-squares regression line to all shoreline positions through time.

$$D_{i,t} = \beta_0 + \beta_1 t + \epsilon$$

where β_1 represents the LRR value for transect i. Negative LRR values indicate long-term shoreline retreat, and positive values indicate long-term shoreline advancement.

The descriptive statistics of SCE, NSM, EPR, and LRR were calculated to provide an initial overview of shoreline behaviour. In the analysed sector, NSM ranged from -1159.84 m to +965.38 m, EPR ranged from -38.76 m yr^-1 to +32.26 m yr^-1, and LRR ranged from -44.46 m yr^-1 to +36.01 m yr^-1. These values indicate strong spatial variability and justify the need for spatial statistical analysis rather than reliance on average change rates alone.

2.5. Spatial autocorrelation analysis using Moran's I

To determine whether shoreline change indicators were randomly distributed or spatially clustered along the coastline, Global Moran's I was applied to the DSAS-derived NSM, EPR, and LRR values. Moran's I is a global spatial autocorrelation statistic that evaluates the degree to which similar values occur near one another in space (Moran, 1950).

$$I = (n / S_0) * [\sum_i \sum_j w_{ij} (x_i - \bar{x})(x_j - \bar{x})] / [\sum_i (x_i - \bar{x})^2]$$

where n is the number of transects, x_i and x_j are shoreline change values at transects i and j, $\bar{x}$ is the mean value of the variable, w_{ij} is the spatial weight between transects i and j, and S_0 is the sum of all spatial weights.

Because the shoreline data were organised as regularly spaced transects at 50-m intervals, spatial relationships were defined along the baseline using a fixed-distance neighbourhood. This approach is appropriate for shoreline datasets because neighbouring transects are expected to be influenced by similar local geomorphological and hydrodynamic conditions. A positive and statistically significant Moran's I value indicates that similar erosion or accretion values are spatially clustered, whereas a value close to zero indicates a random pattern.

In this study, Moran's I was calculated separately for NSM, EPR, and LRR to assess whether shoreline displacement, annual change rate, and long-term trend exhibited spatial clustering. The statistical significance of Moran's I was evaluated using z-scores and permutation-based significance testing.

2.6. Erosion and accretion hotspot analysis using Getis-Ord Gi*

After testing global spatial autocorrelation, local hotspot analysis was conducted using the Getis-Ord Gi* statistic (Getis & Ord, 1992; Ord & Getis, 1995). While Moran's I indicates whether the overall shoreline change pattern is clustered, Getis-Ord Gi* identifies the specific locations of statistically significant clusters.

$$G_i^* = [\sum_j w_{ij} x_j - \bar{x} \sum_j w_{ij}] / [S \sqrt{((n \sum_j w_{ij}^2 - (\sum_j w_{ij})^2)/(n - 1))}]$$

where x_j is the shoreline change value at transect j, w_{ij} is the spatial weight between transects i and j, n is the number of transects, $\bar{x}$ is the mean value, and S is the standard deviation.

For shoreline change interpretation, the sign and magnitude of the DSAS indicators were considered carefully. Since negative NSM, EPR, and LRR values represent erosion, the hotspot analysis was interpreted in terms of erosion-dominated and accretion-dominated clusters. Statistically significant clusters of negative shoreline change values were classified as erosion hotspots, whereas statistically significant clusters of positive values were classified as accretion hotspots.

The Gi* outputs were interpreted using standard confidence levels: 90% confidence level for weak clusters, 95% confidence level for significant clusters, and 99% confidence level for highly significant clusters. A fixed alongshore neighbourhood distance of approximately 500 m was used in the hotspot analysis. Given the 50-m transect spacing, this neighbourhood distance was suitable for identifying kilometre-scale erosion and accretion clusters while reducing isolated transect-level noise.

2.7. Shoreline vulnerability zonation framework

A GIS-based shoreline vulnerability zonation framework was developed by integrating DSAS-derived shoreline change indicators and spatial statistical outputs. The purpose of this step was to transform numerical shoreline change values into management-oriented vulnerability classes. The general logic follows established coastal vulnerability assessment approaches in which geomorphological and process-based indicators are integrated to identify relatively more vulnerable coastal segments (Gornitz, 1991; Thieler & Hammar-Klose, 1999; Ramieri et al., 2011).

The vulnerability assessment was based primarily on three shoreline change indicators: LRR, representing the long-term shoreline trend; EPR, representing the annual rate of shoreline change; and NSM, representing the magnitude of net shoreline displacement. Because erosion is represented by negative values, the signed DSAS indicators were converted into erosion-oriented variables before integration. In this way, larger positive transformed values represented greater erosion intensity.

$$NSM'_i = -NSM_i$$

$$EPR'_i = -EPR_i$$

$$LRR'_i = -LRR_i$$

Each transformed indicator was then standardised to allow comparison among variables with different units.

$$Z_{k,i} = (x_{k,i} - \bar{x}_k) / s_k$$

where $Z_{k,i}$ is the standardised score of indicator k at transect i, $x_{k,i}$ is the transformed shoreline change value, $\bar{x}_k$ is the mean, and s_k is the standard deviation.

A composite shoreline vulnerability index was then calculated as follows:

$$SVI_i = 0.35 Z_{LRR',i} + 0.30 Z_{EPR',i} + 0.25 Z_{NSM',i} + 0.10 H_i$$

where SVI_i is the shoreline vulnerability index for transect i, and H_i represents the hotspot significance score derived from Getis-Ord Gi* analysis. Greater weight was assigned to LRR because it represents the long-term shoreline trend, followed by EPR and NSM. The hotspot score was included to give additional importance to transects located within statistically significant erosion clusters.

The final vulnerability classes were defined as follows:

- Very high vulnerability: severe and persistent erosion, negative NSM/EPR/LRR values, and statistically significant erosion hotspot membership;
- High vulnerability: strong erosion tendency in at least two DSAS indicators, with or without moderate hotspot significance;
- Moderate vulnerability: mixed shoreline behaviour or moderate erosion/accretion values;
- Low vulnerability / relatively stable zone: limited shoreline movement or non-significant long-term change; and
- Accretion-dominated zone: positive shoreline displacement and statistically significant accretion clustering.

This classification allowed the identification of management-priority shoreline segments where erosion-control measures, field monitoring, or land-use restrictions may be required.

2.8. Uncertainty assessment

Uncertainty assessment is essential in shoreline change studies because extracted shoreline positions may be affected by image resolution, georeferencing error, tidal conditions, seasonal variability, classification error, and shoreline definition. In this study, uncertainty was evaluated using the DSAS uncertainty-related outputs, including EPR uncertainty and the confidence interval associated with regression-based shoreline change estimates.

The forecasting and DSAS output dataset included uncertainty-related parameters such as EPRunc, LCI90, and regression goodness-of-fit statistics. These outputs were used to support the interpretation of shoreline change rates and to distinguish persistent trends from uncertain or weak changes. The EPR uncertainty value was considered when interpreting annual shoreline change rates, while the LRR confidence interval was used to assess the reliability of long-term erosion or accretion trends.

In addition, visual inspection of the extracted shoreline positions was carried out to reduce classification errors associated with shallow water, muddy flats, and wet intertidal surfaces. Although Landsat imagery provides an effective long-term archive for shoreline monitoring, its 30-m spatial resolution imposes limitations on detecting very small shoreline changes. Therefore, the results were interpreted at the segment and hotspot scale rather than as isolated transect-level changes. The complete methodological framework is shown in Figure 2.

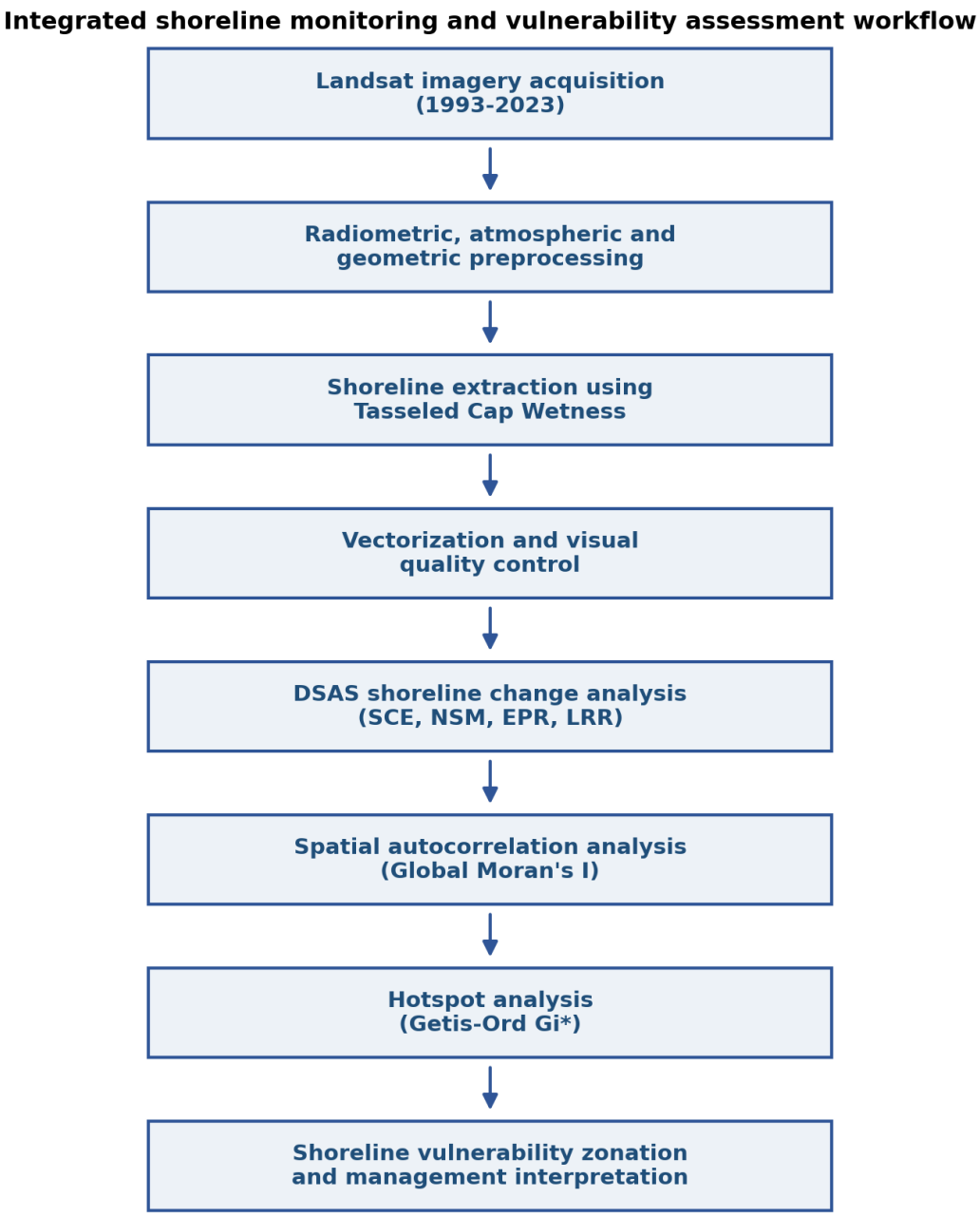


Figure 2. Methodological framework of the integrated shoreline monitoring, hotspot analysis, and vulnerability zonation approach.

3. Results

3.1. General characteristics of shoreline change indicators

The DSAS-based shoreline change analysis was conducted along 350 shore-normal transects, corresponding to transect IDs 201 to 550, along the Khor-e Seh Deyreh-Bandar Genaveh coastal sector. The transects were spaced at 50-m intervals, allowing the detection of detailed alongshore variability in shoreline behaviour. Four

shoreline change indicators, including SCE, NSM, EPR, and LRR, were analysed to describe the magnitude, direction, annual rate, and long-term trend of shoreline movement.

The descriptive statistics of the DSAS-derived indicators reveal substantial spatial variability along the study coastline. The Shoreline Change Envelope (SCE) ranged from 12.99 m to 1159.84 m, with a mean value of 344.02 m, indicating that some coastal segments experienced very large positional fluctuations during the study period. The Net Shoreline Movement (NSM) varied from -1159.84 m to +965.38 m, with a mean value of -132.92 m, suggesting that shoreline retreat was dominant overall. The End Point Rate (EPR) ranged from -38.76 m yr^-1 to +32.26 m yr^-1, with a mean value of -4.44 m yr^-1. Similarly, the Linear Regression Rate (LRR) ranged from -44.46 m yr^-1 to +36.01 m yr^-1, with a mean value of -4.84 m yr^-1. A consolidated summary of these statistics is provided in Table 1.

These results indicate that the coastline did not behave uniformly during the 1993-2023 period. Instead, shoreline movement was characterised by a mosaic of erosion-dominated, accretion-dominated, and relatively stable segments. The negative mean values of NSM, EPR, and LRR indicate an overall tendency toward shoreline retreat, but the wide range of values confirms that this general trend masks strong local contrasts.

[Insert Table 1 here]

Table 1. Descriptive statistics of DSAS-derived shoreline change indicators along the study area

Indicator	Minimum	Maximum	Mean	Median
SCE (m)	12.99	1159.84	344.02	263.71
NSM (m)	-1159.84	+965.38	-132.92	-107.45
EPR (m yr^-1)	-38.76	+32.26	-4.44	-3.59
LRR (m yr^-1)	-44.46	+36.01	-4.84	-4.21

Note: Positive values indicate shoreline advancement or accretion, while negative values indicate shoreline retreat or erosion.

3.2. Net Shoreline Movement pattern

The NSM results show that shoreline displacement varied considerably along the study coastline. Out of the 350 analysed transects, 248 transects showed negative NSM values, indicating shoreline retreat, while 102 transects showed positive NSM values, indicating shoreline advancement. This means that approximately 70.9% of the transects experienced net retreat during the 1993-2023 period, whereas 29.1% experienced net advancement.

The maximum shoreline retreat was -1159.84 m, while the maximum shoreline advancement was +965.38 m. Such a wide range of NSM values indicates that shoreline changes were not gradual or spatially uniform. Instead, large displacements were concentrated in specific coastal segments. The strongest negative NSM values were associated with erosion-dominated sections, whereas the strongest positive NSM values were mainly related to depositional zones, particularly near tidal inlets, shallow intertidal flats, and sediment accumulation areas (Figure 3).

The dominance of negative NSM values suggests that shoreline retreat has been the prevailing process along much of the Khor-e Seh Deyreh-Bandar Genaveh coastal sector. However, the presence of substantial positive NSM values confirms that accretion was also significant in several segments, reinforcing the need for spatially explicit analysis rather than reliance on average change values alone.

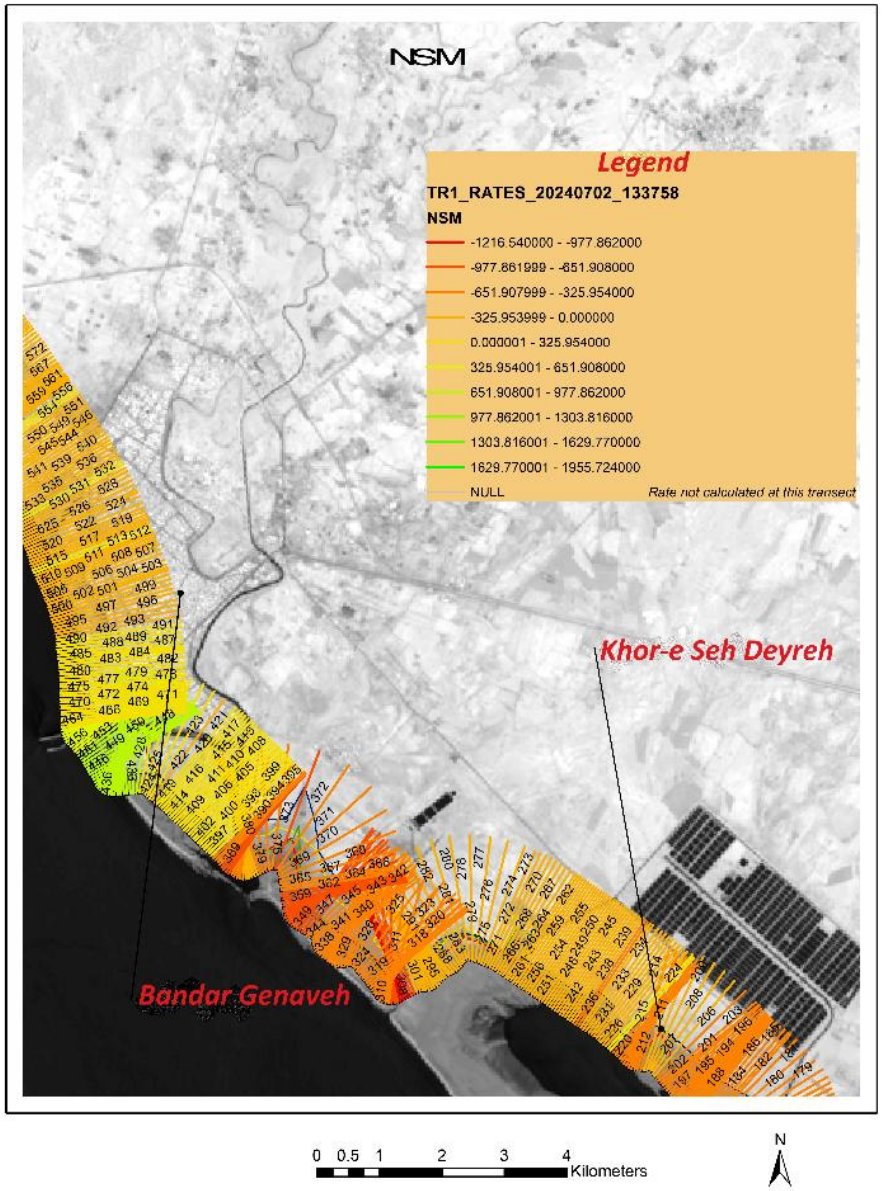


Figure 3. Spatial distribution of Net Shoreline Movement (NSM) along the study coastline from 1993 to 2023.

3.3. End Point Rate pattern

The EPR values provide an estimate of the annual shoreline change rate between the oldest and most recent shoreline positions. The results show that 248 transects had negative EPR values, 101 transects had positive EPR values, and one transect showed a near-zero value. The EPR ranged from -38.76 m yr^-1 to +32.26 m yr^-1, indicating strong contrasts between erosion and accretion rates along the coastline.

The mean EPR value of -4.44 m yr^-1 confirms that, at the scale of the entire analysed sector, erosion was the dominant process. Nevertheless, the simultaneous presence of high positive and high negative EPR values demonstrates that the annual shoreline change rate varied sharply along the coast (Figure 4). This pattern

suggests that some coastal segments have undergone persistent retreat, while others have experienced active sediment accumulation.

The EPR pattern is generally consistent with the NSM distribution, as erosion-dominated transects also tend to show negative annual rates. However, because EPR is calculated only from the first and last shoreline positions, it may be more sensitive to episodic changes and short-term fluctuations. Therefore, EPR was interpreted together with LRR to distinguish short-term or endpoint-controlled behaviour from persistent long-term shoreline trends.

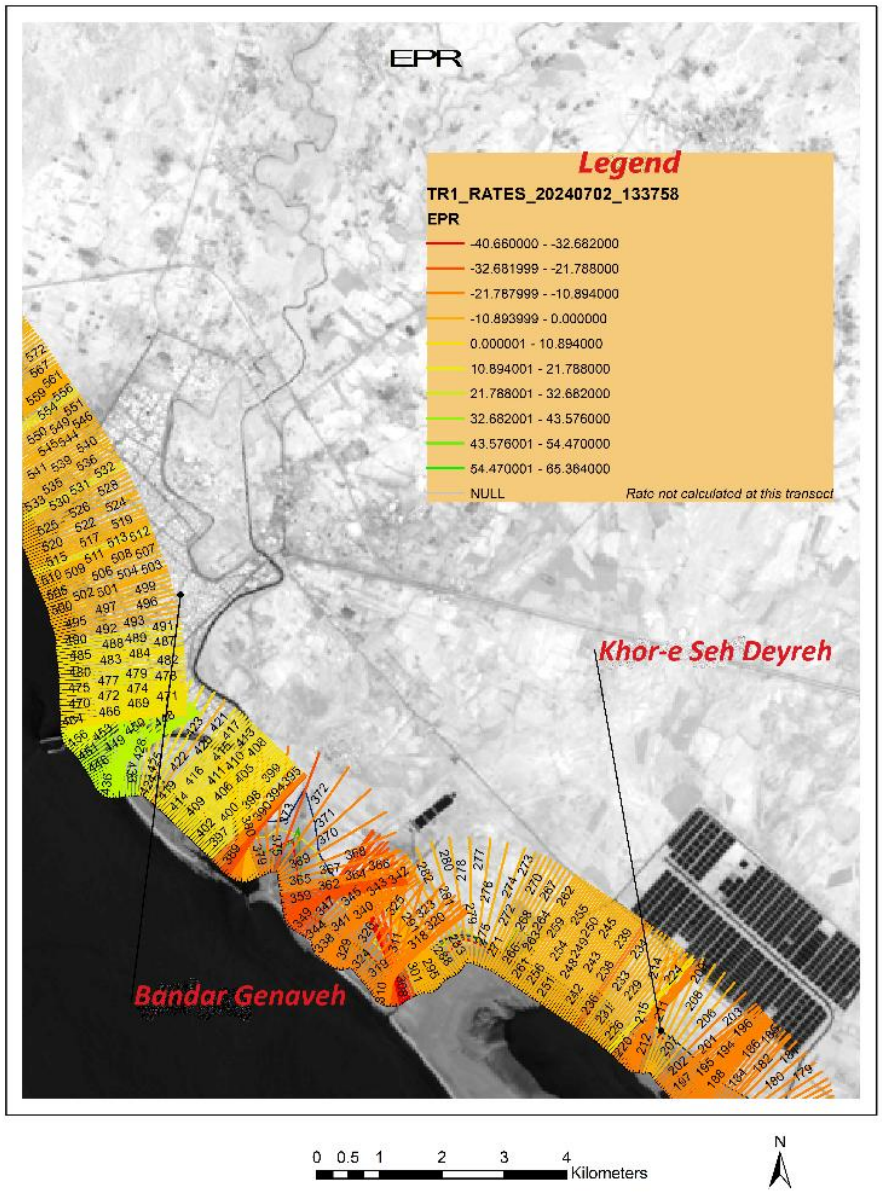


Figure 4. Spatial distribution of End Point Rate (EPR) along the study coastline from 1993 to 2023.

3.4. Long-term shoreline trend based on LRR

The LRR results provide a more robust representation of long-term shoreline behaviour because they are calculated using all available shoreline positions through time. The LRR values ranged from -44.46 m yr^-1 to +36.01 m yr^-1, with a mean value of -4.84 m yr^-1. Among the 350 transects, 218 transects showed negative LRR values, 130 transects showed positive LRR values, and two transects were close to zero.

Compared with NSM and EPR, the LRR indicator showed a slightly lower number of erosion-dominated transects, but the mean value remained negative. This indicates that although some transects may have experienced temporal fluctuations, the dominant long-term tendency of the study coastline was retreat (Figure 5). The strongest negative LRR values were concentrated in specific erosion-prone segments, whereas positive LRR values were mainly concentrated in accretion-dominated zones.

The comparison between EPR and LRR indicates that some shoreline segments experienced short-term or endpoint-sensitive changes, while others showed persistent long-term trends. This distinction is important because management decisions should be based not only on the magnitude of displacement but also on the persistence of shoreline change through time.

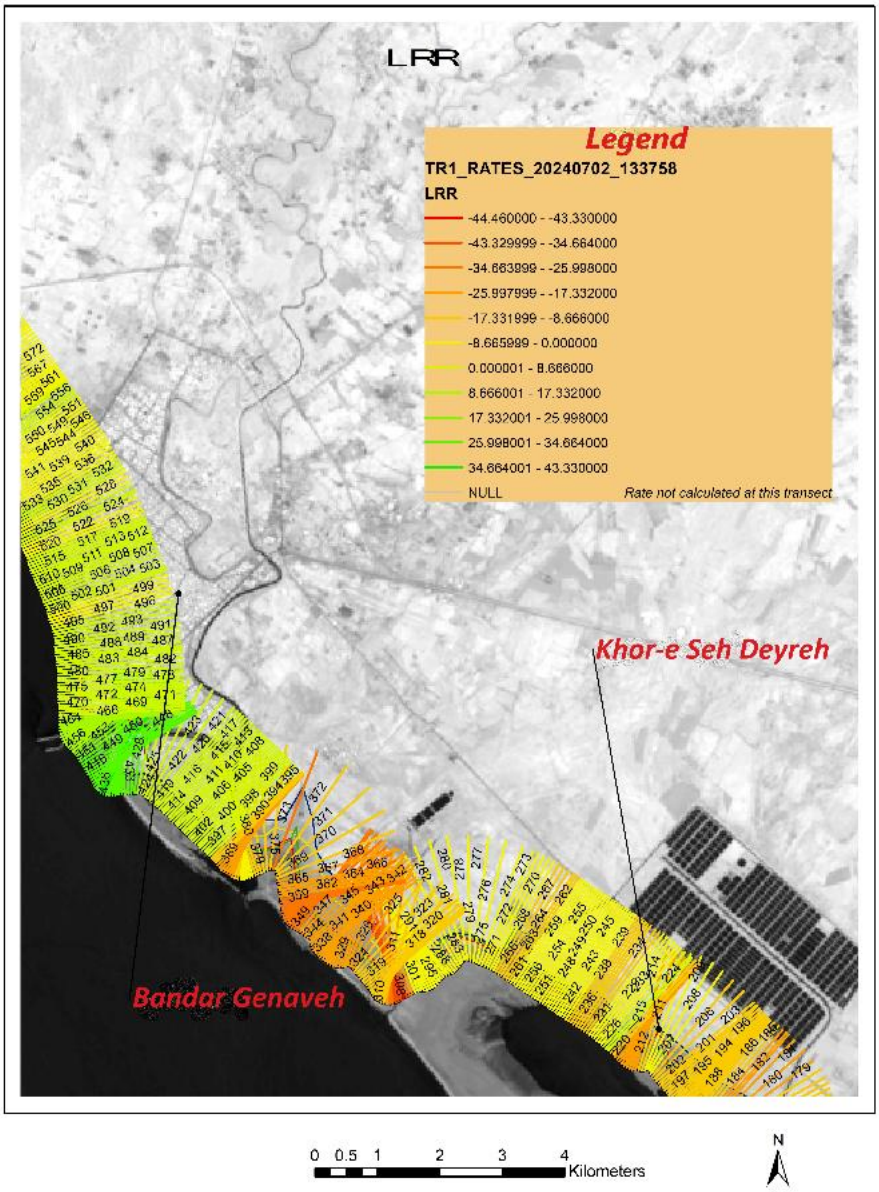


Figure 5. Spatial distribution of Linear Regression Rate (LRR) along the study coastline from 1993 to 2023.

3.5. Spatial autocorrelation of shoreline change indicators

Global Moran's I was calculated for NSM, EPR, and LRR to determine whether shoreline changes were randomly distributed or spatially clustered along the coastline. The results show strong positive spatial autocorrelation for all three indicators. Moran's I values were 0.862 for NSM, 0.862 for EPR, and 0.865 for LRR. These values indicate that similar shoreline change values were strongly clustered along the study coastline. The complete Global Moran's I results are reported in Table 2.

The positive and statistically significant Moran's I values confirm that erosion and accretion did not occur randomly. Instead, shoreline change indicators were spatially organised into clusters of similar behaviour. This finding is important because it supports the central argument of the study: shoreline change along the northern

Persian Gulf should not be interpreted only through mean rates or isolated transect values. Rather, its spatial structure must be analysed to identify erosion hotspots, accretion clusters, and management-priority zones.

[Insert Table 2 here]

Table 2. Global Moran's I results for shoreline change indicators

Indicator	Moran's I	Significance	Interpretation
NSM	0.862	p <= 0.001	Strong clustered pattern
EPR	0.862	p <= 0.001	Strong clustered pattern
LRR	0.865	p <= 0.001	Strong clustered pattern

The LRR indicator showed the highest Moran's I value among the three indicators. Therefore, LRR was considered the most appropriate primary indicator for identifying persistent erosion and accretion hotspots, while NSM and EPR were used as supporting indicators.

3.6. Erosion and accretion hotspots

The Getis-Ord Gi* analysis was applied to identify local clusters of statistically significant erosion and accretion. The results revealed two main erosion hotspots and one major accretion hotspot along the study coastline. The principal erosion and accretion hotspot ranges are summarised in Table 3.

The first erosion hotspot was identified between transects 204 and 220. This segment represents a localised but significant erosion-prone zone in the initial part of the study area. The second and more extensive erosion hotspot was identified between transects 294 and 393. This segment forms the dominant erosion cluster of the study area and represents the most important management-priority zone for shoreline retreat.

In contrast, a major accretion hotspot was detected between transects 406 and 490. This segment is characterised by positive shoreline change values and represents a depositional zone where shoreline advancement has been dominant. The location of this accretion cluster suggests the influence of sediment accumulation processes, probably associated with tidal inlet dynamics, shallow intertidal flats, and reduced hydrodynamic energy. The main hotspot results are summarised in Table 3 and illustrated in Figure 6.

[Insert Table 3 here]

Table 3. Main erosion and accretion hotspots identified by Getis-Ord Gi* analysis

Hotspot type	Transect range	Approximate length	Interpretation
Erosion hotspot	204-220	~0.85 km	Localised significant erosion zone
Erosion hotspot	294-393	~5.00 km	Main erosion-prone coastal segment
Accretion hotspot	406-490	~4.25 km	Main sediment accumulation zone

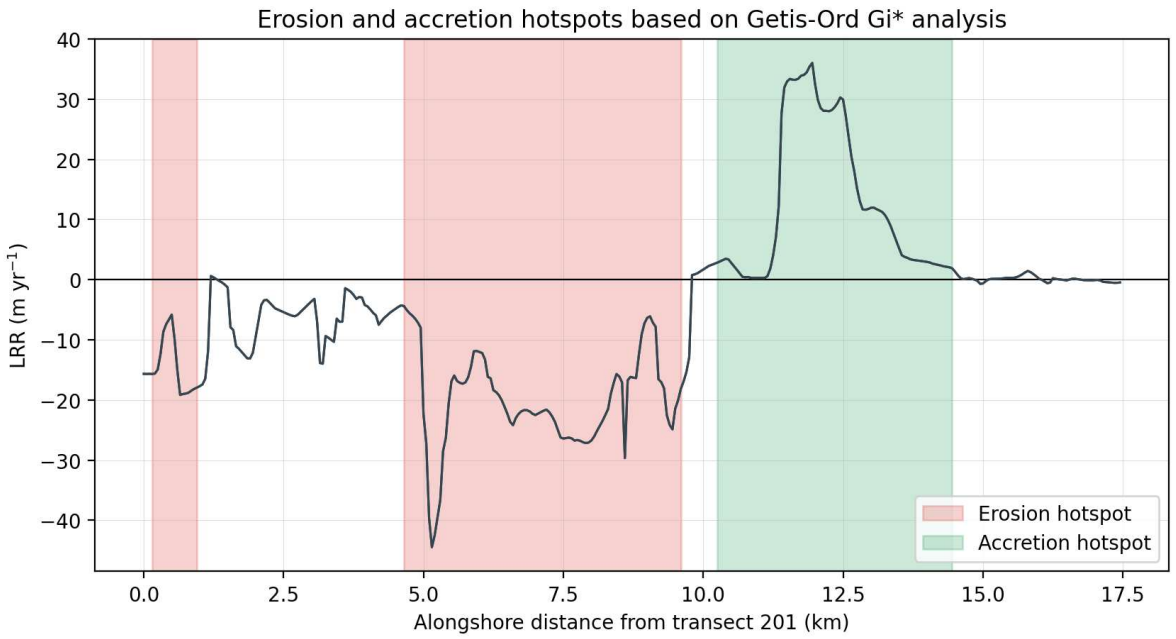


Figure 6. Erosion and accretion hotspots based on Getis-Ord Gi analysis using LRR as the primary long-term shoreline change indicator.*

The hotspot analysis demonstrates that the strongest shoreline changes are spatially concentrated rather than randomly distributed. This confirms that combining DSAS outputs with spatial statistics provides a more meaningful interpretation of shoreline dynamics than conventional rate-based analysis alone.

3.7. Shoreline vulnerability zones

The shoreline vulnerability zonation was developed by integrating the DSAS-derived indicators with the spatial statistical outputs. The results indicate that the study coastline can be divided into several management-relevant zones: very high vulnerability zones, high vulnerability zones, moderate vulnerability zones, relatively stable zones, and accretion-dominated zones.

The very high vulnerability zones correspond mainly to the statistically significant erosion hotspots, especially transects 204-220 and 294-393. These segments are characterised by persistent negative LRR values, high negative NSM and EPR values, and spatial clustering of erosion. Therefore, they should be considered priority areas for coastal monitoring, field verification, and erosion-control planning.

The high vulnerability zones include shoreline segments adjacent to the main erosion hotspots where retreat is still evident but the statistical significance or intensity of clustering is lower. These areas may represent transitional zones that could become more unstable if sediment supply decreases or human interventions intensify. The moderate vulnerability zones are characterised by mixed shoreline behaviour, where erosion and accretion indicators are not consistently dominant. These areas require periodic monitoring because they may shift toward erosion or accretion depending on hydrodynamic and sedimentary conditions.

The low vulnerability or relatively stable zones include transects with limited shoreline movement and weak long-term change. The accretion-dominated zone, mainly corresponding to transects 406-490, is characterised by positive shoreline movement and significant clustering of accretion. Although this zone is not erosion-prone, it remains important from a coastal management perspective because excessive sediment accumulation

can affect tidal inlet morphology, navigation, habitat conditions, and local sediment balance. The final zonation is shown in Figure 7.

Overall, the vulnerability zonation confirms that the Khor-e Seh Deyreh-Bandar Genaveh shoreline is not a uniform coastal system. Instead, it consists of spatially organised erosion and accretion zones that require different management responses.

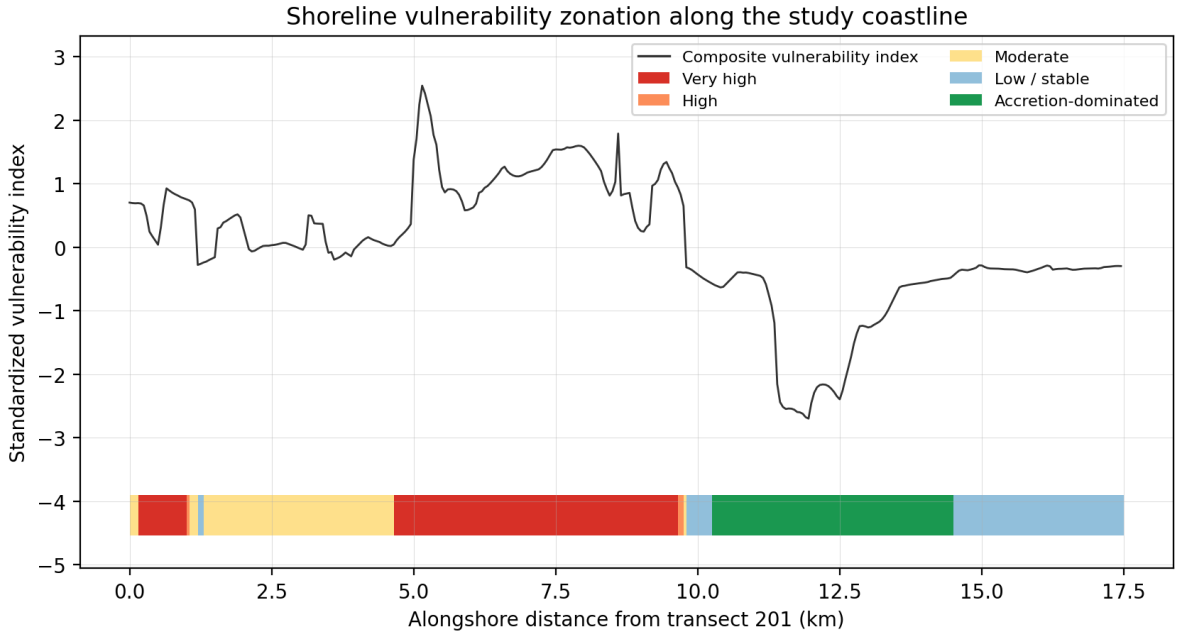


Figure 7. Shoreline vulnerability zonation along the study coastline derived from DSAS indicators and hotspot significance.

4. Discussion

4.1. Spatial heterogeneity of shoreline change

The results of this study demonstrate that shoreline change along the northern Persian Gulf is highly heterogeneous and cannot be adequately explained by average retreat or accretion rates alone. Although the mean values of NSM, EPR, and LRR indicate an overall erosional tendency along the Khor-e Seh Deyreh-Bandar Genaveh coastal sector, the wide range of values reveals strong local contrasts in shoreline behaviour. The coexistence of severe retreat, marked shoreline advancement, and relatively stable segments over short alongshore distances indicates that the study area behaves as a spatially complex coastal system rather than a uniform shoreline unit.

This finding is consistent with previous shoreline change studies showing that coastal erosion and accretion are strongly controlled by local geomorphological, hydrodynamic, sedimentary, and anthropogenic conditions. In particular, semi-enclosed coastal systems, tidal inlets, muddy intertidal flats, and human-modified shorelines often exhibit highly variable responses to similar regional forcing conditions. Therefore, the interpretation of shoreline change only through mean values may obscure critical segments where erosion is severe and persistent.

The results also show that the spatial organisation of shoreline change is statistically meaningful. Global Moran's I values of approximately 0.862-0.865 for NSM, EPR, and LRR confirm strong positive spatial autocorrelation. This means that similar erosion or accretion values tend to occur near one another, forming

spatially organised clusters rather than random transect-level variations. This result is important because it provides statistical support for the existence of erosion hotspots and accretion-dominated zones along the study coastline.

4.2. Interpretation of erosion hotspots

The Getis-Ord Gi* analysis identified two major erosion hotspots: a relatively localised erosion hotspot between transects 204-220 and a more extensive erosion hotspot between transects 294-393. These segments represent the most critical parts of the study coastline from the perspective of shoreline retreat and vulnerability.

The first erosion hotspot, although shorter in length, indicates a concentrated zone of significant shoreline retreat. Such localised erosion may be associated with site-specific factors such as shoreline geometry, local wave exposure, sediment imbalance, or the influence of nearby human interventions. Because this hotspot is spatially compact, it may require detailed field verification to identify the precise local controls responsible for the observed retreat.

The second erosion hotspot, extending approximately 5 km, is the dominant erosion-prone segment of the study area. Its spatial continuity suggests that erosion in this part of the coast is not the result of isolated transect-level fluctuations but reflects a persistent geomorphological and sedimentary process. The coincidence of negative NSM, EPR, and LRR values in this segment indicates both substantial shoreline displacement and a persistent long-term retreat trend. Therefore, this zone should be considered the primary management-priority area for erosion monitoring and coastal protection planning.

The presence of these erosion hotspots may be related to several interacting factors. Open-coast segments are generally more exposed to wave action and longshore sediment transport, which can intensify shoreline retreat where sediment supply is insufficient. In addition, human interventions such as small piers, coastal structures, shoreline modifications, and aquaculture-related land-use changes may alter local sediment pathways and contribute to erosion in adjacent sections. However, because the present study is based primarily on remote sensing and DSAS-derived indicators, these causal interpretations should be supported in future work by field observations, hydrodynamic data, sediment transport analysis, and high-resolution coastal morphology surveys.

4.3. Interpretation of accretion-dominated zones

In contrast to the erosion hotspots, the Getis-Ord Gi* analysis identified a major accretion hotspot between transects 406-490. This segment is characterised by positive shoreline change values and statistically significant clustering of shoreline advancement. The presence of this accretion-dominated zone confirms that the study coast is not undergoing uniform retreat; rather, erosion and deposition occur simultaneously in different parts of the coastal system.

The accretion hotspot is likely associated with depositional conditions near tidal inlets, shallow intertidal flats, and low-energy coastal environments. Such settings can act as sediment traps, particularly where tidal currents, reduced wave energy, and fine-grained sediment availability favour sediment accumulation. In muddy and shallow coastal environments of the Persian Gulf, shoreline advancement may also be influenced by tidal-flat expansion, sediment redistribution, and local modifications to water circulation.

From a management perspective, accretion-dominated zones should not be interpreted simply as low-risk areas. Although they are not erosion hotspots, they may still have important environmental and operational implications. Excessive sediment accumulation can modify tidal inlet morphology, affect water exchange, alter habitat conditions, influence navigation in shallow coastal waters, and change the sediment balance of adjacent

shoreline segments. Therefore, accretion zones should be included in long-term coastal monitoring programs together with erosion-prone areas.

4.4. Added value of spatial statistics in shoreline change assessment

One of the main contributions of this study is the integration of DSAS-derived shoreline change indicators with spatial statistical analysis. Conventional shoreline change studies often report NSM, EPR, and LRR values independently or summarise them using mean rates. While these indicators are useful, they do not necessarily reveal whether shoreline changes are spatially organised, clustered, or randomly distributed.

The application of Moran's I and Getis-Ord Gi* addresses this limitation. Moran's I demonstrated that shoreline change indicators exhibit strong spatial autocorrelation, while Getis-Ord Gi* identified the specific locations of statistically significant erosion and accretion clusters. This combination transforms DSAS outputs from descriptive transect-level statistics into spatially explicit information that is more useful for environmental monitoring and coastal management.

The results show that LRR is particularly useful for detecting persistent long-term shoreline behaviour, while NSM and EPR provide complementary information on total displacement and endpoint-based annual change rates. The slightly different behaviour of these indicators confirms that relying on only one metric may lead to incomplete interpretation. For example, EPR may be more sensitive to the first and last shoreline positions, whereas LRR incorporates all shoreline positions and therefore provides a more stable estimate of long-term trend. The combined use of NSM, EPR, LRR, and spatial statistics therefore provides a stronger basis for identifying priority coastal segments.

4.5. Shoreline vulnerability zonation and management implications

The vulnerability zonation developed in this study provides a practical framework for translating shoreline change indicators into management-oriented classes. The very high vulnerability zones correspond mainly to the statistically significant erosion hotspots, especially transects 204-220 and 294-393. These areas combine strong negative shoreline change values with spatial clustering of erosion, making them priority areas for coastal monitoring, field investigation, and erosion-control planning.

High vulnerability and moderate vulnerability zones represent transitional shoreline segments where erosion is present but less intense or less spatially significant. These zones are important because they may become more unstable if sediment supply decreases, coastal development expands, or hydrodynamic forcing intensifies. Low vulnerability or relatively stable zones, on the other hand, may not require immediate intervention but should remain part of periodic monitoring programs.

The proposed zonation has direct implications for coastal management in the northern Persian Gulf. First, it helps identify where limited monitoring and protection resources should be prioritised. Second, it provides a spatial basis for regulating coastal development in erosion-prone areas. Third, it can support decisions about where field surveys, sediment sampling, or hydrodynamic modelling should be focused. Finally, it offers a repeatable framework that can be updated when new satellite images or shoreline data become available.

In this sense, the study moves beyond conventional shoreline change detection and provides an applied regional coastal monitoring framework. Rather than only describing how much the shoreline has changed, the method identifies where shoreline change is spatially concentrated and which coastal segments require management attention.

4.6. Limitations and future research

Although the integrated approach used in this study improves the interpretation of shoreline change patterns, several limitations should be acknowledged. First, the analysis is based on Landsat imagery, whose 30-m spatial resolution is suitable for long-term regional monitoring but may not capture small-scale shoreline fluctuations. Therefore, the results should be interpreted at the segment and hotspot scale rather than as precise transect-level field measurements.

Second, shoreline extraction in tidal and muddy coastal environments is inherently challenging. Wet sediments, shallow water, tidal flats, and seasonal moisture variations can affect the position of the detected land-water boundary. Although the Tasseled Cap Wetness component and visual quality control improved shoreline extraction, future research should incorporate tidal correction, higher-resolution imagery, UAV surveys, or field GPS measurements to further validate extracted shoreline positions.

Third, the present study identifies spatial patterns and statistically significant clusters, but it does not directly model the physical mechanisms responsible for erosion and accretion. Future work should integrate wave climate, tidal currents, sediment characteristics, bathymetry, coastal slope, land-use change, and hydrodynamic modelling to explain the causal processes behind the detected hotspots.

Finally, the vulnerability zonation framework can be further improved by incorporating additional environmental and socio-economic variables, such as distance to infrastructure, land use, coastal elevation, population exposure, ecological sensitivity, and protection status. Combining shoreline change indicators with these variables would allow the development of a more comprehensive coastal vulnerability index for the northern Persian Gulf.

Overall, the results confirm that the integration of Landsat-based shoreline monitoring, DSAS-derived indicators, Moran's I, Getis-Ord Gi* hotspot analysis, and vulnerability zonation provides a robust and practical approach for identifying erosion-prone and management-priority coastal segments in data-scarce regions.

5. Conclusions

This study developed an integrated framework for assessing coastal erosion hotspots and shoreline vulnerability along the northern Persian Gulf using multi-temporal Landsat imagery, DSAS-derived shoreline change indicators, and spatial statistical analysis. Shoreline positions from 1993 to 2023 were extracted using the Tasseled Cap Wetness component, and shoreline change was quantified along 350 shore-normal transects spaced at 50-m intervals. The analysis focused on four shoreline change indicators, including SCE, NSM, EPR, and LRR, to evaluate the magnitude, direction, annual rate, and long-term trend of shoreline movement.

The results showed that the Khor-e Seh Deyreh-Bandar Genaveh coastal sector experienced substantial spatial variability during the study period. The NSM values ranged from -1159.84 m to +965.38 m, while EPR and LRR ranged from -38.76 to +32.26 m yr^-1 and from -44.46 to +36.01 m yr^-1, respectively. The negative mean values of NSM, EPR, and LRR indicate that shoreline retreat was the dominant overall process along the study coast. However, the wide range of positive and negative values confirms that the shoreline did not behave uniformly and that erosion, accretion, and relative stability occurred simultaneously over short alongshore distances.

The spatial statistical results demonstrated that shoreline changes were not randomly distributed. Global Moran's I values for NSM, EPR, and LRR were approximately 0.862-0.865, indicating strong positive spatial autocorrelation and confirming that similar shoreline change values were spatially clustered. The Getis-Ord Gi* analysis identified two main erosion hotspots, located mainly between transects 204-220 and 294-393, and

one major accretion hotspot between transects 406-490. These findings show that the most critical shoreline changes were concentrated in specific coastal segments rather than being evenly distributed along the coastline.

The shoreline vulnerability zonation further translated the DSAS and spatial statistical outputs into management-oriented classes. The very high vulnerability zones corresponded mainly to the statistically significant erosion hotspots, particularly the extensive erosion-prone segment between transects 294-393. These areas should be considered priority zones for field verification, continuous monitoring, erosion-control planning, and regulation of future coastal development. In contrast, the accretion-dominated zone between transects 406-490 represents an important depositional segment that should also be monitored because sediment accumulation can influence tidal inlet morphology, habitat conditions, navigation, and sediment balance in adjacent areas.

The main contribution of this study is that it moves beyond conventional shoreline change assessment based only on rate calculation. By integrating DSAS-derived indicators with Moran's I, Getis-Ord Gi* hotspot analysis, and GIS-based vulnerability zonation, the study provides a spatially explicit regional marine coastal monitoring framework for identifying erosion-prone and management-priority shoreline segments. This approach is particularly useful for data-scarce coastal regions where long-term field monitoring is limited but historical satellite imagery is available.

Although the proposed framework provides valuable insights into shoreline dynamics, several limitations should be considered. The analysis was based on Landsat imagery with moderate spatial resolution, and shoreline extraction in muddy, shallow, and tidal environments may be affected by tidal stage, wet sediment, and classification uncertainty. Future studies should integrate higher-resolution satellite imagery, UAV surveys, field GPS measurements, tidal correction, sediment data, wave and current information, and hydrodynamic modelling to better explain the physical mechanisms controlling the detected erosion and accretion hotspots. Incorporating socio-economic and ecological exposure indicators would also allow the development of a more comprehensive coastal vulnerability index for the northern Persian Gulf.

Overall, the findings demonstrate that combining long-term satellite-based shoreline monitoring with spatial statistics and vulnerability zonation can provide a robust and practical basis for coastal environmental assessment, erosion-risk management, and sustainable shoreline planning along the northern Persian Gulf.

References

Abdul Maulud, K. N., Selamat, S. N., Mohd, F. A., Md Noor, N., Wan Mohd Jaafar, W. S., Kamarudin, M. K. A., Ariffin, E. H., Adnan, N. A., & Ahmad, A. (2022). Assessment of shoreline changes for the Selangor Coast, Malaysia, using the Digital Shoreline Analysis System technique. Urban Science, 6(4), 71. https://doi.org/10.3390/urbansci6040071

Anselin, L. (1995). Local indicators of spatial association-LISA. Geographical Analysis, 27(2), 93-115. https://doi.org/10.1111/j.1538-4632.1995.tb00338.x

Boak, E. H., & Turner, I. L. (2005). Shoreline definition and detection: A review. Journal of Coastal Research, 21(4), 688-703. https://doi.org/10.2112/03-0071.1

Chen, C., Fu, J., Zhang, S., & Zhao, X. (2019). Coastline information extraction based on the tasseled cap transformation of Landsat-8 OLI images. Estuarine, Coastal and Shelf Science, 217, 281-291. https://doi.org/10.1016/j.ecss.2018.10.021

Colak, A. T. I. (2024). Geospatial analysis of shoreline changes in the Oman coastal region (2000-2022) using GIS and remote sensing techniques. Frontiers in Marine Science, 11, 1305283. https://doi.org/10.3389/fmars.2024.1305283

Darwish, K., & Smith, S. (2023). Landsat-based assessment of morphological changes along the Sinai Mediterranean coast between 1990 and 2020. Remote Sensing, 15(5), 1392. https://doi.org/10.3390/rs15051392

Fisher, A., Flood, N., & Danaher, T. (2016). Comparing Landsat water index methods for automated water classification in eastern Australia. Remote Sensing of Environment, 175, 167-182. https://doi.org/10.1016/j.rse.2015.12.055

Getis, A., & Ord, J. K. (1992). The analysis of spatial association by use of distance statistics. Geographical Analysis, 24(3), 189-206. https://doi.org/10.1111/j.1538-4632.1992.tb00261.x

Gittman, R. K., Fodrie, F. J., Popowich, A. M., Keller, D. A., Bruno, J. F., Currin, C. A., Peterson, C. H., & Piehler, M. F. (2015). Engineering away our natural defenses: An analysis of shoreline hardening in the United States. Frontiers in Ecology and the Environment, 13(6), 301-307. https://doi.org/10.1890/150065

Gornitz, V. (1991). Global coastal hazards from future sea level rise. Palaeogeography, Palaeoclimatology, Palaeoecology, 89(4), 379-398. https://doi.org/10.1016/0031-0182(91)90173-O

Himmelstoss, E. A., Henderson, R. E., Kratzmann, M. G., & Farris, A. S. (2021). Digital Shoreline Analysis System (DSAS) version 5.1 user guide. U.S. Geological Survey Open-File Report 2021-1091. https://doi.org/10.3133/ofr20211091

Khakhim, N., Kurniawan, A., Pranowo, W. S., Khasanah, E. U., & Halilintar, P. (2024). Shoreline morphological change prognostic model based on spatiotemporal framework imagery data on the northern coast of Java, Indonesia. Kuwait Journal of Science, 51, 100274. https://doi.org/10.1016/j.kjs.2024.100274

Khurram, S., Pour, A. B., Bagheri, M., Helmy Ariffin, E., Akhir, M. F., & Bahri Hamzah, S. (2025). Satellite-based multi-decadal shoreline change detection by integrating deep learning with DSAS: Eastern and southern coastal regions of Peninsular Malaysia. Remote Sensing, 17(19), 3334. https://doi.org/10.3390/rs17193334

Kumar Das, S., Sajan, B., Ojha, C., & Soren, S. (2021). Shoreline change behavior study of Jambudwip Island of Indian Sundarban using DSAS model. The Egyptian Journal of Remote Sensing and Space Sciences, 24(3), 961-970. https://doi.org/10.1016/j.ejrs.2021.09.004

Moran, P. A. P. (1950). Notes on continuous stochastic phenomena. Biometrika, 37(1/2), 17-23. https://doi.org/10.1093/biomet/37.1-2.17

Nylén, T., Calle, M., & Gonzales-Inca, C. (2025). Unveiling coastal change across the Arctic with full Landsat collections and data fusion. Remote Sensing of Environment, 322, 114696. https://doi.org/10.1016/j.rse.2025.114696

Ord, J. K., & Getis, A. (1995). Local spatial autocorrelation statistics: Distributional issues and an application. Geographical Analysis, 27(4), 286-306. https://doi.org/10.1111/j.1538-4632.1995.tb00912.x

Ramieri, E., Hartley, A., Barbanti, A., Santos, F. D., Gomes, A., Hilden, M., Laihonen, P., Marinova, N., & Santini, M. (2011). Methods for assessing coastal vulnerability to climate change. European Topic Centre on Climate Change Impacts, Vulnerability and Adaptation, Technical Paper 1/2011.

Sekar, L. G., Androws, X., Annaidasan, K., Kumar, A., Kannan, R., Muthusankar, G., & Balasubramani, K. (2024). Assessment of shoreline changes and associated erosion and accretion pattern in coastal watersheds of Tamil Nadu, India. Natural Hazards Research, 4(2), 231-238. https://doi.org/10.1016/j.nhres.2023.09.008

Sunder, S., Ramsankaran, R., & Ramakrishnan, B. (2017). Inter-comparison of remote sensing-based shoreline mapping techniques at different coastal stretches of India. Environmental Monitoring and Assessment, 189, 290. https://doi.org/10.1007/s10661-017-5996-1

Sun, W., Chen, C., Liu, W., Yang, G., Meng, X., Wang, L., & Ren, K. (2023). Coastline extraction using remote sensing: A review. GIScience & Remote Sensing, 60(1), 2243671. https://doi.org/10.1080/15481603.2023.2243671

Thieler, E. R., & Hammar-Klose, E. S. (1999). National assessment of coastal vulnerability to sea-level rise: Preliminary results for the U.S. Atlantic Coast. U.S. Geological Survey Open-File Report 99-593.

Thomas, G. A. J., Santha Ravindranath, R. R., Jeyagopal, S., & Thodhal Yoganandham, S. (2023). Statistical analysis of shoreline change reveals erosion and baseline are increasing off the northern Tamil Nadu coasts of India. Environmental Monitoring and Assessment, 195, 409. https://doi.org/10.1007/s10661-023-11015-0

Zeinali, S., Dehghani, M., Rastegar, M. A., & Mojarrad, M. (2017). Detecting shoreline changes in Chabahar Bay by processing satellite images. Scientia Iranica, Transactions A: Civil Engineering, 24(4), 1802-1809.

Zorlu, O., & Kusak, L. (2025). An assessment of the long-term change of the Mersin west coastline using digital shoreline analysis system and detection of pattern similarity using fuzzy C-means clustering. Frontiers in Marine Science, 12, 1457016. https://doi.org/10.3389/fmars.2025.1457016

Supplementary Files

This is a list of supplementary files associated with this preprint. Click to download.

- 05DeclarationofCompetingInterest1.docx